The Journal of Chemical Physics

Electron transfer mediated decay in $HeLi_2$ cluster: Potential energy surfaces and decay widths

Cite as: J. Chem. Phys. **150**, 164309 (2019); https://doi.org/10.1063/1.5082952
Submitted: 26 November 2018 . Accepted: 09 April 2019 . Published Online: 30 April 2019

Aryya Ghosh, Lorenz S. Cederbaum, and Kirill Gokhberg

The Journal of Chemical Physics ARTICLE scitation.org/journal/jcp

Electron transfer mediated decay in $HeLi_2$ cluster: Potential energy surfaces and decay widths

Cite as: J. Chem. Phys. 150, 164309 (2019); doi: 10.1063/1.5082952
Submitted: 26 November 2018 • Accepted: 9 April 2019 •
Published Online: 30 April 2019

Aryya Ghosh, Lorenz S. Cederbaum, and Kirill Gokhberg

AFFILIATIONS

Theoretische Chemie, Physikalisch-Chemisches Institut, Universität Heidelberg, Im Neuenheimer Feld 229, D-69120 Heidelberg, Germany

ABSTRACT

Electron transfer mediated decay (ETMD) is a process responsible for double ionization of dopants in He droplets. It is initiated by producing He^+ in the droplet, which is neutralized by ETMD, and has been shown to strongly enhance the dopant's double ionization cross section. The efficiency of ETMD, the spectra of emitted secondary electrons, and the character of the ionic products depend on the nuclear dynamics during the decay. To date, there has been no theoretical investigation of multimode dynamics which accompanies ETMD, which could help to understand such dynamics in a He droplet. In this article, we consider the He–Li_2 cluster where an *ab initio* examination of multimode dynamics during the electronic decay is feasible. Moreover, this cluster can serve as a minimal model for Li_2 adsorbed on the droplet's surface—a system where ETMD can be observed experimentally. In He droplets, Li_2 can be formed in both the ground $X^1\Sigma_g^+$ and the first excited $a^3\Sigma_u^+$ states. In this article, we present *ab initio* potential energy surfaces of the electronic states of the He–Li_2 cluster involved in ETMD, as well as the respective decay widths. We show that the structure of these surfaces and expected nuclear dynamics strongly depend on the electronic state of Li_2. Thus, the overall decay rate and the appearance of the observable electron spectra will be dictated by the electronic structure of the dopant.

I. INTRODUCTION

Superfluid ^{4}He droplets are a unique and versatile spectroscopic embedding medium used for isolation, cooling, and study of atoms, molecules, and their aggregates.[1,2] Since the droplets are transparent to electromagnetic radiation below 21 eV, such photons are directly absorbed by the dopants which leads to their vibrational or electronic excitation.[3–5] The photons of energies above 21 eV can be absorbed by the droplets themselves, which leads to the excitation or ionization of the He atoms. The photoabsorption cross section of a droplet, whose average size varies between 10^3 and 10^{12} atoms,[2] is much larger than the dopant's. Therefore, the energy is first absorbed by the droplet and is afterward transferred in an interatomic process to the dopant which usually leads to its ionization. Several processes responsible for such indirect ionization of the dopant have been identified to date. Thus, excited He atoms may ionize a dopant in the excitation transfer ionization[6–8] or Penning ionization processes,[2,9] whereby an excited He atom relaxes transferring the excess energy to a dopant and ionizing it. The interaction between the He^+ cation and a dopant may lead to the electron transfer from the latter to the former.[10] The ionization via charge transfer usually results in electronically excited dopant cations due to the energy conservation requirement.[10–12] However, for rare gas (RG) dopants,[13] whose ionized excited states have high energies so that the He^+-RG and He-RG^{+*} states cannot be brought into resonance, radiative charge transfer[14,15] and production of the dopant cation in its ground state is the most probable mechanism.

If the double ionization potential of the dopant is below the electron affinity of He^+ (24.6 eV), another electron transfer process, electron transfer mediated decay (ETMD),[16] becomes possible. In it, the excess energy released in the electron transfer from the dopant is used to eject another dopant's electron into the continuum. ETMD is common in weakly bound chemical systems; it was observed in rare gas clusters[17–19] and salt solutions.[20] In rare gas clusters, it proceeds on a time scale of a few picoseconds,[21] while in microsolvated clusters, it becomes as fast as a few tens of femtoseconds.[22,23] Whenever energetically allowed, it is, therefore, the dominant charge transfer mechanism in weakly bound chemical media. *Ab initio*

calculations demonstrated that in He environment, the ionization of a helium atom followed by ETMD becomes a potent mechanism for doubly ionizing the dopant species already in the presence of a few He neighbors.[24] Subsequent photoelectron-photoion coincidence measurements showed that double ionization of Mg clusters embedded in He droplets proceeded, within the experimental uncertainty, solely by ETMD.[25] ETMD can also account for the previously reported double ionization by He^+ ions of C_{60}-H_2O complexes[26,27] embedded in nanodroplets, although the mechanism could not be deduced unequivocally from the experimental data.

ETMD is a purely electronic process and will occur even if the nuclei are fixed. However, in rare gas clusters, characteristic vibrational frequencies in the decaying state are larger than the ETMD rate in the Franck-Condon region, and the decay is accompanied by nuclear dynamics. They substantially increase the decay rate and strongly affect the spectra of emitted electrons.[21,28] Moreover, it has been previously shown that in charge transfer reactions inside the droplets, the He^+ ion is steered toward an electron rich moiety in the dopant, and this steering is responsible for the location of the ionization site and the following chemical transformations of the ionized dopant.[11,12] Such steering might also be important in the case of ETMD and impact its rate and the distribution of the products. Despite their importance, the nuclear dynamics which accompany ETMD were studied in detail only for a diatomic cluster and involved only one nuclear coordinate.[21] The dynamics during ETMD in He droplets will actively involve several coordinates and require a polyatomic model.

A suitable model for studying the multidimensional dynamics of ETMD in He droplets has been suggested by the droplets doped with the dimers of alkali atoms (Ak_2) which are adsorbed on the droplet's surface.[29–31] In this work, we discuss the particular example of Li_2, the system which has been previously studied both as a free molecule (see Ref. 32 and references therein) and as an adsorbate on the surface of He droplets.[33,34] Like the hydrogen atom, the Li atom has a single valence electron. However, unlike H_2, where the first excited state is dissociative, both the ground $X^1\Sigma_g^+$ and the first excited $a^3\Sigma_u^+$ states of Li_2 are bound.[32] In the ground state, the two valence electrons form a strong single bond so that it is appropriate to think about Li_2 in this state as a molecule. However, the binding in the excited state is only due to the dispersive interaction and is so weak that one is dealing with a van der Waals dimer. The 20-fold discrepancy in the binding energies of the two states affects the relative abundances of the triplet and singlet Li_2 formed on the He droplet's surface. The formation of the Li dimer on the surface is accompanied by its cooling via evaporating of He atoms. Since the binding energies of Li_2 to the He droplet are of order of a few millielectron volts,[35] and the energy dissipated in the cooling of the singlet Li_2 is much larger than in the case of the triplet, the former has higher probability of desorbing from the surface. As a result, the spin triplet Li_2 adsorbates predominate.[29,34] However, the exact ratio of the high to low spin dimers is sensitive to the droplet's size and can be varied.[36]

The dimer in both electronic spin states can undergo ETMD with He^+. Since these states correspond to very different electronic structures of Li_2 and different orientations of the dimer relative to the He droplet's surface—perpendicular for the singlet, parallel for the triplet[37]—we expect an observable difference in the impact of nuclear dynamics in these two states on ETMD. One can obtain a useful insight in the dynamics of ETMD by considering a minimal He–Li_2 system which is amenable to high level *ab initio* calculations. Indeed, following the ionization of the droplet, ETMD takes place between Li_2 and He^+ or He_2^+ which is produced following the fast self-trapping of the hole.[10] The neutral He atoms in the droplet play two roles during the decay. First, they form a steric constraint on the dynamics of the Li_2–He_n^+ subsystem. Second, they serve as a heat sink dissipating the vibrational energy in the ETMD state concurrently with the electronic decay. The impact of these two effects can be estimated, for example, by comparing the experimental ETMD electron spectra with their benchmark counterparts. Apart from being the model for a more complex system, the $HeLi_2$ cluster is of interest by itself, since it allows a detailed *ab initio* investigation of the impact of multimode nuclear dynamics make on the electronic decay.

In this article, we present the results of the *ab initio* calculations of the complex potential energy surfaces (PESs) of the ETMD He^+–$Li_2(^1\Sigma_g^+, ^3\Sigma_u^+)$ states, as well as the PESs of the initial He–$Li_2(^1\Sigma_g^+, ^3\Sigma_u^+)$ and final He–Li^+–Li^+ states. We derive and discuss qualitative estimates of ETMD dynamics, rate, and spectra from these PECs. The results of full quantum dynamics calculations of ETMD observables, which use the presented electronic data as the input, will be reported in the follow-up publication.

II. COMPUTATIONAL DETAILS

A. Potential energy surfaces

To represent the three-dimensional potential energy surfaces and the decay widths, we use Jacobi coordinates: the Li–Li distance, r ($0 < r < \infty$), the distance from He to Li_2 center-of-mass, R ($0 < r < \infty$), and the angle between the Li_2 molecular axis and the line connecting its center-of-mass to He, θ ($0 < \theta < \pi/2$) (see Fig. 1).

The computation of the three-dimensional potential energy surfaces (PESs) of the ground ($^1\Sigma_g^+$) and the first excited ($^3\Sigma_u^+$) states of neutral $HeLi_2$ is very challenging due to the exceedingly weak helium-lithium interaction. Their accurate description

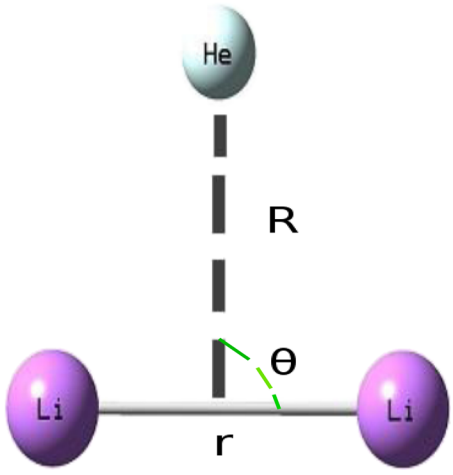

FIG. 1. Jacobi coordinates used to represent the geometry of the $HeLi_2$ cluster.

requires high level *ab initio* methods, as well as carefully chosen basis sets. We computed the PES of the $HeLi_2(^1\Sigma_g^+)$ state using the coupled cluster singles, doubles and perturbative triples [CCSD(T)] method as implemented in the GAMESS-US software package[38,39] and the restricted Hartree-Fock (RHF) reference state. To find an appropriate basis set, we computed the energy along two one-dimensional cuts of the total PES. The cuts were obtained by keeping the Li atoms at the equilibrium distance of isolated Li_2 and varying the distance between He and the center of mass of Li_2 in the linear and T-shaped geometries of the trimer. The cc-pVXZ (X = D,T,Q,5) and aug-cc-pVXZ (X = D,T,Q,5) Dunning basis sets were used on both He and Li atoms. The convergence was achieved for both series of the basis sets at the 5Z level; however, the energies and geometries corresponding to the global potential minima were different for the XZ and aXZ basis sets. The results obtained at the cc-pV5Z level show good agreement with the previously reported theoretical results by Varandas and Brandão[40] and Fuchs and Toennies[41] (see Table I). Therefore, we chose the cc-pV5Z basis set to compute the PES of the $HeLi_2(^1\Sigma_g^+)$ state.

The PES of the first excited state, $HeLi_2(^3\Sigma_u^+)$, was computed by the completely renormalized coupled-cluster method with singles, doubles, and noniterative triples [CR-CC(2,3)] as implemented in the GAMESS-US software package[42] and using the restricted open-shell Hartree Fock (ROHF) reference state. To choose the appropriate basis set for the computation of the corresponding PES, we again studied the basis set convergence using cc-pVXZ (X = D,T,Q,5) series. From our study, we observed that cc-pVXZ (X = D,T,Q,5) series converge at the 5Z level and the cc-pV5Z basis set was used on He and Li atoms. To the best of our knowledge, the PES of this state has not been reported in the literature.

The PESs of the highly excited, singly ionized $He^+Li_2(^1\Sigma_g^+)$ and $He^+Li_2(^3\Sigma_u^+)$ decaying states were computed using the full configuration interaction (FCI) method as implemented in the GAMESS-US package using the RHF ground state of $HeLi_2$ as the reference. The important advantage of the FCI method, as applied to weakly bound systems, is that it is size consistent. The FCI calculations of the complete three-dimensional PES of a resonance state lying in the electronic continuum with all 7 electrons active are computationally expensive. Therefore, in our calculations, we froze the core (1s) orbitals of both lithium atoms which left only three active electrons in the system.

To check the accuracy of this approximation, we computed the binding energy in the $He^+Li_2(^1\Sigma_g^+)$ state at the equilibrium geometry given in Table II. We observed that the energies obtained using a frozen core approximation deviate by less than 1 meV from the ones obtained in the full calculation. In addition, we computed the binding energies using CI-SDT method with the Davidson correction and all seven electrons active, which should take account of the polarization of Li 1s electrons. For the geometries where the decay is prominent, the difference in binding energies amounted to a few tens of millielectron volts. Such deviation would result in a negligible error in the ETMD electron spectra which are characterized by broad (≈1 eV) peaks. While it proved to be impossible to obtain similar results for the $He^+Li_2(^3\Sigma_u^+)$ state, the results discussed above and the calculations in the He^+Li dimer indicate that the effect of unfreezing of the 1s electrons on the electron spectra will be negligible.

The highly excited He^+Li_2 states are embedded into the continuum and interact with it forming metastable electronic resonance states. The PESs of such states are, in general, complex with the complex part being equal to the half of the decay width.[43] Since the Gaussian atomic basis sets are used in the computations, the continuum states are discretized, and calculating the real part of the PES can be done straightforwardly as if the state were electronically bound. However, care should be taken in selecting the basis set. Increasing the basis set on the lithium atoms improves the description of interaction energy. However, it also increases the density of pseudocontinuum in the energy range of interest. Interaction of many pseudocontinuum states with the decaying state complicates the energy spectrum and makes the construction of the real part of the PES a difficult task. Keeping this in mind, we used the aug-cc-pVTZ basis set on the helium atom and the cc-pVTZ basis set on the lithium atoms. Additional 2s, 2p, 2d Rydberg-like Kaufmann-Baumeister-Jungen (KBJ)-type basis functions[44] were added to the basis sets on He and Li. These basis sets are accurate enough as can be seen from sufficiently accurate equilibrium Li–Li distances and binding energies in isolated Li_2 in the electronic states of interest. Moreover, they allow the efficient computation and construction of the real parts of the three-dimensional resonance He^+Li_2 PES.

The PES of the final state of the ETMD process, $Li^+(2s^{-1})HeLi^+(2s^{-1})$, was again computed using the FCI method with the 1s orbitals of the Li atoms frozen. We used the aug-cc-pVTZ basis set on the helium atom and cc-pVTZ basis set on the lithium atoms. Additional 2s, 2p, 2d Rydberg-like KBJ-type basis functions were added to the helium and lithium atoms.

TABLE I. Theoretical equilibrium geometries and binding energies of $HeLi_2(^1\Sigma_g^+)$ and $HeLi_2(^3\Sigma_u^+)$ states. The binding energies are obtained relative to the energy of the separated He atom and Li_2 molecule at its corresponding equilibrium geometry.

	R (Å)	r (Å)	θ (deg)	D_e (meV)
$HeLi_2(^1\Sigma_g^+)$[a]	6.91	2.69	0	0.22
$HeLi_2(^1\Sigma_g^+)$[b]	6.75	2.69	0	0.26
$HeLi_2(^1\Sigma_g^+)$[c]	6.88	2.69	0	0.22
$HeLi_2(^1\Sigma_g^+)$[d]	6.85	2.69	0	0.20
$HeLi_2(^3\Sigma_u^+)$[a]	5.42	4.18	90	0.41

[a]This work—CCSD(T), cc-pV5Z basis set.
[b]This work—CR-CC(2,3), aug-cc-pV5Z basis set.
[c]Reference 40.
[d]Reference 41.

TABLE II. Equilibrium geometries of the $He^+Li_2(^1\Sigma_g^+)$ and $He^+Li_2(^3\Sigma_u^+)$ decaying states computed by FCI. The binding energies are obtained relative to the energy of the separated He^+ ion and Li_2 molecule at the corresponding equilibrium geometry.

	R (Å)	r (Å)	θ (deg)	D_e (eV)
$He^+Li_2(^1\Sigma_g^+)$	3.0	2.90	90	1.33
$He^+Li_2(^3\Sigma_u^+)$	0	7.20	...	1.27

B. Electronic decay widths

The ETMD widths were computed using the Fano-Stieltjes method[45] which we briefly review below. In the theory of resonances developed by Fano and Feshbach,[46–48] the resonance wavefunction is represented as a superposition of the bound (Φ) and the continuum ($\chi_{\beta,\epsilon}$) components. The total decay width Γ is calculated using the coupling term between the bound and continuum parts,

$$\Gamma = 2\pi \sum_{\beta} |\langle \phi | H | \chi_{\beta,\epsilon} \rangle|^2, \tag{1}$$

where H denotes the full electronic Hamiltonian and β enumerates open decay channels. The asymptotic kinetic energy of the ETMD electron, ϵ, can be estimated from the expression $\epsilon \approx E_r - E_\beta$, where E_r is the real part of the resonance energy and E_β is the energy of the final state β.

In the Fano-Feshbach formalism, the division of the resonance state into bound and continuum parts is done by partitioning of the Hilbert space into the subspace P of the final continuum states, and the subspace Q of the closed channels which contains the bound part of the resonance. The subspaces P and Q satisfy the following conditions:

$$P + Q = 1, PQ = 0. \tag{2}$$

The bound part of the resonance can be obtained through diagonalization of the electronic Hamiltonian projected onto the Q space

$$QHQ|\Phi\rangle = E_b|\phi\rangle, \tag{3}$$

where the energy E_b is approximately equal to E_r for narrow resonances. The diagonalization of the electronic Hamiltonian projected onto the P subspace produces the continuum states which enter the width calculations

$$PHP|\chi_{\beta,\epsilon}\rangle = E_\beta|\chi_{\beta,\epsilon}\rangle. \tag{4}$$

Since the L^2 basis set is used in representing H, Eq. (4) produces not a true continuum but discrete pseudocontinuum states which have wrong normalization and asymptotic behavior. To obtain the accurate numerical value and correct dimensionality of the decay width Γ, we employed the Stieltjes imaging technique.[45,49]

To construct the matrix representation of H and its projections onto the P and Q subspaces, we used the extended second order algebraic diagrammatic construction [ADC(2)x] scheme for the Green's function [defined within the space spanned by the one-hole (1h) and two-hole one particle (2h1p) configurations].[50,51] In this approach, the coupling between the 1h configurations is treated to second order of perturbation theory, while the coupling between the 1h and 2h1p configurations and between the 2h1p configurations is treated to first order of perturbation theory. To construct the P subspace, we considered the two-hole-one-particle (2h1p) configurations which represent the final doubly ionized state with an outgoing free electron. The hole orbitals used in the construction of the P subspace are the $2\sigma_g$ and $2\sigma_u$ valence orbitals of Li_2. Therefore, the P subspace contains all possible $2\sigma_i^{-1}2\sigma_j^{-1}b^1$ configurations, where b refers to a virtual orbital. The hole orbitals used in the construction of the Q subspace are the 1s orbital of the He atom and the $2\sigma_{g,u}$ orbitals of Li_2 such that the Q subspace comprises $1s_{He}^{-1}$, $1s_{He}^{-1}2\sigma_{g,u}^{-1}b^1$, and $1s_{He}^{-2}b^1$ configurations. The Q subspace also contains the bound parts of resonance states of the He^*–Li_2^+ character. The lowest of them, $He^*(1s2s^3S)$–Li_2^+, interacts with the $He^+Li_2(^3\Sigma_u^+)$ state as discussed below.

The calculation of the decay widths was carried out by first using the MOLCAS quantum chemistry package[52] for computing the restricted Hartree-Fock (RHF) reference state and two-electron integrals. Later on, our in-house ADC(2)x code for the Green's function was used to compute the ETMD width. The decay width calculations were performed using the cc-pVTZ basis set on the helium and lithium atoms. For an improved description of the pseudocontinuum, additional 4s, 4p, 4d continuumlike Kaufmann-Baumeister-Jungen basis functions were added to the helium and lithium atoms. We checked the convergence of the width with respect to the basis set by further augmenting the latter with the KBJ functions. This led to the variation of the width within 5% from the value obtained using the original basis set.

III. RESULTS AND DISCUSSION

The ETMD process which leads to the double ionization of Li_2 in the presence of He is summarized in the following equation:

$$h\nu + HeLi_2 \rightarrow He^+Li_2 + e_{photo} \rightarrow HeLi^+Li^+ + e_{photo} + e_{ETMD}. \tag{5}$$

In Eq. (5), we assumed that He^+ was produced in photoionization, although the same ETMD process can be also initiated by electron impact ionization. Initially, the cluster can be either in its ground electronic state $HeLi_2(^1\Sigma_g^+)$ or in the first excited electronic state $HeLi_2(^3\Sigma_u^+)$. Ionization of He promotes the ground state system to the $He^+Li_2(^1\Sigma_g^+)$ ($S = 1/2$) state, while the excited state is promoted to either $He^+Li_2(^3\Sigma_u^+)$ ($S = 1/2$) or $He^+Li_2(^3\Sigma_u^+)$ ($S = 3/2$) state. ETMD is energetically allowed for all three states; however, spin conservation rules allow ETMD only in the two spin-doublet decaying states, while it is forbidden within a nonrelativistic approach for the spin-quartet state. Since the spin-orbit coupling is small for the light atoms comprising the cluster, only the first two states will be discussed below. Their decay proceeds to the single final $HeLi^+Li^+$ state which subsequently undergoes Coulomb explosion into either the $HeLi^+/Li^+$ or $He/Li^+/Li^+$ channel.

The kinetic energies of the ETMD electrons and the ionic fragments are the experimental observables. Their accurate computation requires taking into account the nuclear dynamics during the decay. The essential input to such calculations are the potential energy surfaces (PESs) of the initial, decaying, and final states, as well as the decay widths. In the following, we present the results of *ab initio* calculations of these electronic properties and draw qualitative conclusions as to the appearance of the expected electron and ion spectra.

A. PESs of the initial states

Binding of He to neutral atoms and molecules is extremely weak. The $HeLi_2$ cluster is no exception, and to understand its structure, it is advantageous to consider first the isolated Li_2 molecule. In its ground state $^1\Sigma_g^+$, this molecule is bound and the experimental bond length and the binding energy are 2.673 Å and 1.056 eV, respectively.[32] The two Li atoms are covalently bound in the $^1\Sigma_g^+$ state with both valence electrons occupying the binding $2\sigma_g$ orbital.

In the first excited $^3\Sigma_u^+$ state, one electron occupies the bonding $2\sigma_g$, while the other the antibonding $2\sigma_u$ orbital. Despite the absence of a covalent bond, the Li_2 molecule remains bound due to the dispersive forces between the two Li atoms. This van der Waals bond is much weaker than the covalent one in the ground state which is reflected in the increased bond length and the diminished binding energy found experimentally to be 4.169 Å and 41.41 meV.[32] Summing up, one may consider Li_2 as a strongly bound molecule in its ground state and as a weakly bound van der Waals cluster in the first excited state.

Adding the He atom perturbs the Li_2 molecule only weakly in both states of interest. Indeed, for the range of geometries for which the bound cluster exists, the deviation of the binding energies and bond lengths of Li_2 from the equilibrium values in the isolated system is negligible. Therefore, to visualize the potential energy surface of the cluster in the two lowest electronic states, one may keep the Jacobi coordinate r constant and equal to the equilibrium Li–Li distance in the corresponding state of the isolated molecule and plot the PES as the function of R and θ alone.

The corresponding surfaces are shown in Fig. 2; we list the respective equilibrium geometries in Table I. In the electronic ground $HeLi_2(^1\Sigma_g^+)$ state, the equilibrium geometry is linear with θ equal to 0, and R = 6.91 Å. The well depth relative to the $He/Li_2(^1\Sigma_g^+)_{eq}$ dissociation limit is D_e = 0.22 meV. These results can be compared to the equilibrium geometries of the $HeLi_2$ electronic ground state obtained by other authors. Thus, the CEPA geometries reported in Ref. 41 give R_0 = 6.87 Å and D_e = 0.2 meV. The double many-body expansion method, where the two- and three-body interaction terms are further subdivided into the Hartree-Fock and correlation contributions, produced R_0 = 6.91 Å and

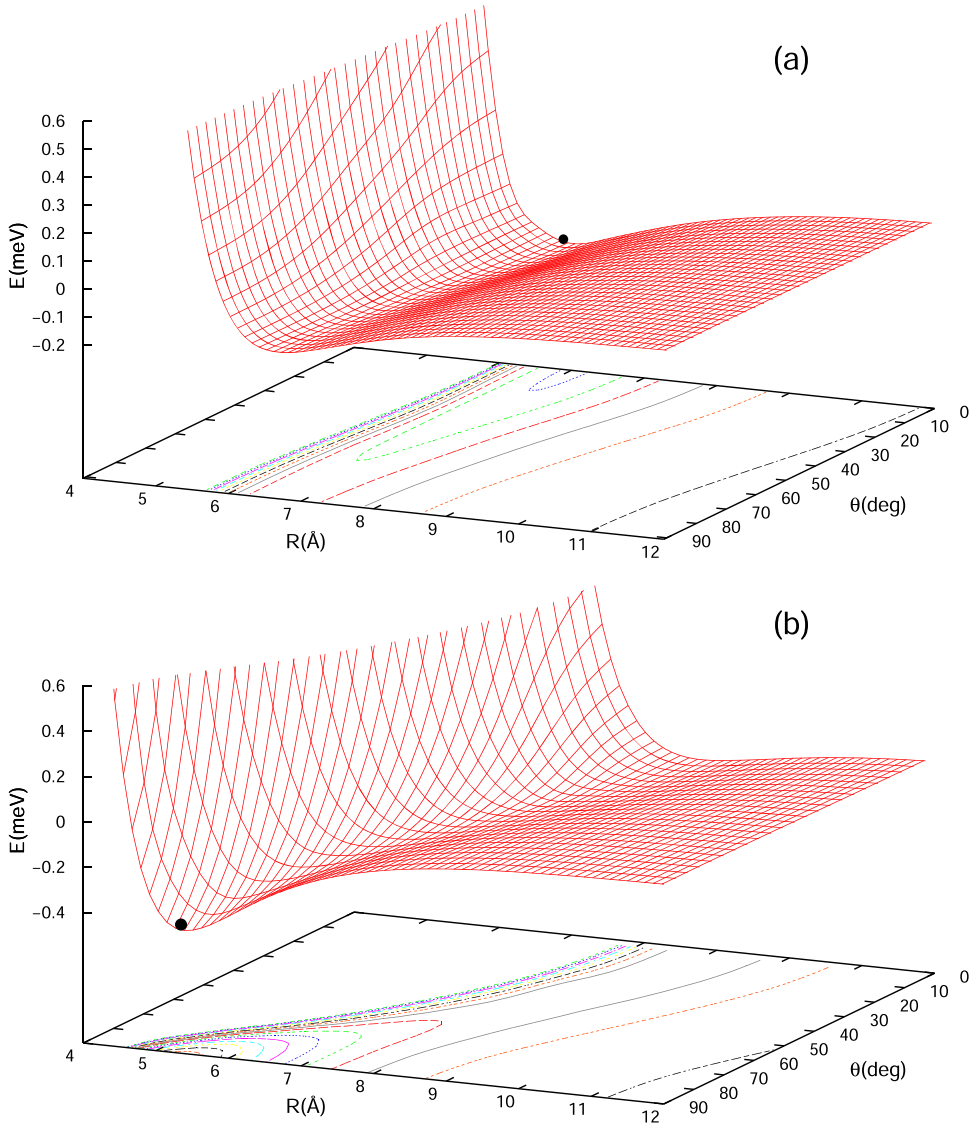

FIG. 2. Two-dimensional potential energy surfaces of the ground $HeLi_2(^1\Sigma_g^+)$ and first excited $HeLi_2(^3\Sigma_u^+)$ states of the $HeLi_2$ cluster. (a) The PES of the ground state was obtained by keeping r at 2.69 Å (Li_2 equilibrium distance in the $^1\Sigma_g^+$ ground state). The zero of energy was set to coincide with the energy at the $He/(Li_2(^1\Sigma_g^+))_{eq}$ dissociation limit. (b) The PES of the first excited state was obtained by keeping r = 4.18 Å (Li_2 equilibrium distance in the first excited $^3\Sigma_u^+$ state). The zero of energy was set to coincide with the energy at the $He/(Li_2(^3\Sigma_u^+))_{eq}$ dissociation limit. The black dot marks the position of the cluster's equilibrium geometry in the respective electronic state.

D_e = 0.22 meV.[40] Our results are in good agreement with these calculations.

The equilibrium geometry in the first excited $HeLi_2(^3\Sigma_u^+)$ state is T-shaped with $\theta = \pi/2$ and R = 5.42 Å, while the well depth is D_e = 0.41 meV. Both the change in the symmetry of the equilibrium geometry from $C_{\infty v}$ in the ground state to C_{2v} in the excited state and change in the location and depth of the potential minima are dictated by the distribution of the valence electron density in the corresponding electronic states of the Li_2 molecule. As we mentioned above, the configuration of the valence electrons, which are responsible for bonding, in the $HeLi_2(^1\Sigma_g^+)$ state is $2\sigma_g^2$, while in the excited $HeLi_2(^3\Sigma_u^+)$ state, it is $2\sigma_g^1 2\sigma_u^1$. The bonding σ_g orbital is mostly located between the Li atoms, while the antibonding σ_u orbital has a node there. Therefore, compared to the total electron density of the two noninteracting Li atoms, the Li_2 molecule in the ground state has excess electron density between the atoms. In the first excited state, the excess density is located just outside the atoms along the molecular axis. The electron-He interaction is strongly repulsive; therefore, the binding of He is stronger along the direction where the electron density on the partner is low.[53]

The system is usually taken from the initial to the decaying state in a sudden photoionization step, which vertically transfers a vibrational wavepacket from one PES to another. Therefore, different equilibrium geometries of the two electronic states of $HeLi_2$ mean different initial vibrational distributions in the nuclear dynamics which accompany the ETMD process.

B. PESs of the decaying states and the final state of ETMD

Unlike neutral He, the He^+ ion binds strongly to the Li_2 molecule. One, therefore, expects shorter He–Li equilibrium distances in the ionized state. Moreover, the ion strongly perturbs the Li_2 molecule. In general, it polarizes Li_2 and weakens the Li–Li bond, which leads to the increase in the Li–Li equilibrium distance. The exact effect of the positive charge of He^+ on the equilibrium geometry strongly depends on the electronic structure of the Li_2 fragment in the respective decaying state. Thus, the global minimum of the $He^+Li_2(^1\Sigma_g^+)$ PES was found at R = 3.0 Å, r = 2.90 Å, and $\theta = \pi/2$. Comparing this equilibrium geometry with the one in the ground state, we notice, first, that the symmetry shifts from the linear to the T-shaped. The C_{2v} symmetry is explained by the fact that the interaction between He^+ and the valence electron density, which is concentrated between the two Li atoms, is attractive, and not repulsive as in the case of neutral He. Second, the distance between the He^+ and the center-of-mass of Li_2 becomes half of what it was in the initial state. Finally, the polarization of Li_2 and the partial charging of the Li atoms lead to the increase in the Li_2 bond length from 2.69 Å to 2.90 Å. The binding energy relative to the $He^+/(Li_2(^1\Sigma_g^+))_{eq}$ limit is 1.33 eV and is much larger than 0.22 meV binding energy in the ground state. One notes, however, that despite the shift in the position of the global minimum and stronger perturbation of the Li_2 molecule in this decaying state, one may still consider this cluster as a He species attached to the Li_2 molecule. The characteristic two-dimensional PES cut with the coordinate r kept constant at 2.90 Å is shown in Fig. 3.

The picture differs in the case of the $He^+Li_2(^3\Sigma_u^+)$ state. Similar considerations of maximizing the attractive interaction between He^+ and the valence electrons of Li_2 predict a linear equilibrium geometry of the cluster. Indeed, the potential energy surface has three minima, and all three correspond to a linear geometry. In the global minimum, He^+ is located at the center of mass of the Li_2 molecule such that R = 0 Å and r = 7.20 Å. The fact that the most stable cluster configuration in this state is with He^+ located between the Li atoms can be understood by comparing the binding energy of $Li_2(^3\Sigma_u^+)$ (41.41 meV) with the much larger binding energy of He^+Li (650 meV). Therefore, in this electronic state, the system consists of two Li atoms bound to a common center—the He^+ ion.

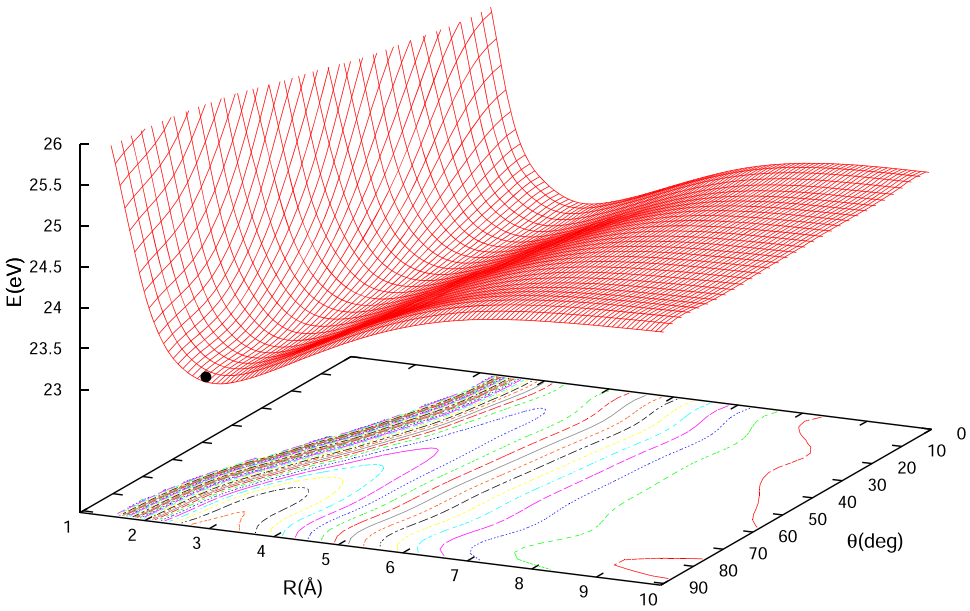

FIG. 3. Two-dimensional potential energy surfaces of the $He^+Li_2(^1\Sigma_g^+)$ state. The shown PES of the $He^+Li_2(^1\Sigma_g^+)$ corresponds to r kept constant at 2.9 Å (Li_2 distance at the global minimum of the respective PES). The zero of energy was set to coincide with the energy at the $He/(Li_2(^1\Sigma_g^+))_{eq}$ dissociation limit. The black dot marks the position of the cluster's equilibrium geometry in the respective electronic state.

The characteristic PES cut with θ held constant at $\pi/2$ is shown in Fig. 4.

There are also a local minimum at R = 5.38 Å, r = 3.16 Å, and θ equals to 0 so that He^+ is located just outside the Li_2 molecule on the molecular axis. The binding energy at the local minimum relative to the $He^+/(Li_2(^3\Sigma_u^+))_{eq}$ dissociation limit is 1.26 eV, while this binding energy for the global minimum is 1.27 eV. Interestingly, the Li–Li interatomic distance at the local minimum of the $He^+Li_2(^3\Sigma_u^+)$ PES is smaller than in the isolated $Li_2(^3\Sigma_u^+)$ molecule. This can be ascribed to the decrease in the electron density in the antibonding $2\sigma_u$ orbital due to the polarization of Li_2 by the He^+ ion. This distance lies closer to the bond length of the $Li_2^+(^2\Sigma_g^+)$ molecular cation (r = 3.09–3.12 Å[54]) than to the one of the isolated $Li_2(^3\Sigma_u^+)$ molecule (r = 4.18 Å).

The final $HeLi^+Li^+$ state of ETMD is dominated by the repulsion between the two Li^+ ions. One might assume from the shape of the PES that the Coulomb explosion in the final state of the ETMD process could lead to the $HeLi^+/Li^+$ channel only when the three atoms are collinear; other configurations should predominantly lead to the three-body $He/Li^+/Li^+$ break-up channel.

C. ETMD widths

The decay width is given by a three-dimensional function of the coordinates. The interplay between its magnitude and the characteristic vibrational frequencies in the decaying state determines at what nuclear configurations the decay will mostly take place. This, in turn, decides the shape of the electron spectra and the overall decay rate. The decay widths in the $He^+Li_2(^1\Sigma_g^+)$ and $He^+Li_2(^3\Sigma_u^+)$ states at the nuclear configurations corresponding to the equilibrium geometries of the respective initial states are 0.0052 meV and 0.0030 meV. The corresponding lifetimes are 130 ps and 220 ps, respectively, and it follows that the ionization and vertical transition of the vibrational wavepacket to the decaying state PES initiates nuclear dynamics which will accompany the decay.

To facilitate the discussion of the computed ETMD widths of the $He^+Li_2(^1\Sigma_g^+)$ and $He^+Li_2(^3\Sigma_u^+)$ states, we present them as cuts along a specific Jacobi coordinate with two other coordinates held constant at the equilibrium values in the corresponding initial state (see Fig. 5). Since the equilibrium geometry of the $HeLi_2(^1\Sigma_g^+)$ state is linear and that of the $HeLi_2(^3\Sigma_u^+)$ is T-shaped, the direct comparison of the widths is of little use; it is their overall behavior which interests us here.

During the decay, the electron is transferred from Li_2 to He^+ along the coordinate R. Therefore, the width should fall off fast (eventually exponentially fast) with increasing R. This is indeed the behavior seen in Figs. 5(a) and 5(a′). The observed variations in Γ with the Li_2 to He distance can be nine orders of magnitude, with largest widths being a few millielectron volts corresponding to the lifetime of a few hundred femtoseconds. The binding along the coordinate R in a decaying state is much stronger than in the corresponding initial state. Therefore, nuclear dynamics which set in after the ionization step will lead to the shortening of the coordinate R accelerating the decay.

The behavior of the widths along the coordinate r in Figs. 5(b) and 5(b′) is dictated by the geometry of the cut. In the linear geometry of the $He^+Li_2(^1\Sigma_g^+)$ state, increasing the Li_2 distance brings one of the Li atoms closer to the He^+, facilitating the charge transfer and increasing the decay width. In the T-shape geometry of the $He^+Li_2(^3\Sigma_u^+)$ state, increasing r leads to the increase in the Li–He^+ distances and to the corresponding decrease in the ETMD width.

More interesting is the dependence of the widths on the angle θ shown in Figs. 5(c) and 5(c′). The decay width should be independent of the angle if the distance between He^+ and the center of

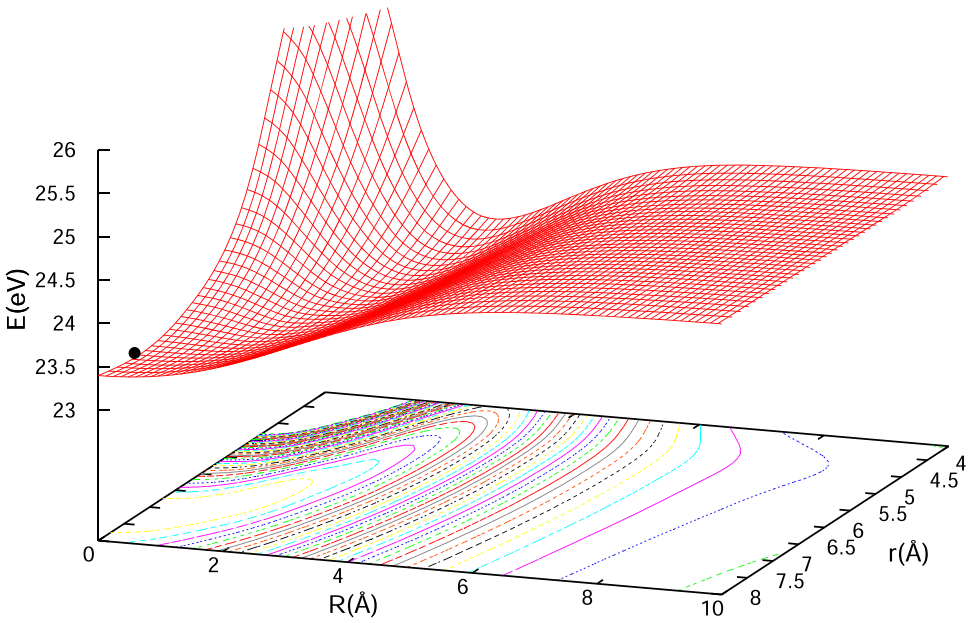

FIG. 4. Two-dimensional potential energy surfaces of the $He^+Li_2(^3\Sigma_u^+)$ state. The shown PES of the $He^+Li_2(^3\Sigma_u^+)$ corresponds to the angle θ kept constant at $\pi/2$. The zero of energy was set to coincide with the energy at the $He/(Li_2(^3\Sigma_u^+))_{eq}$ dissociation limit. The black dot marks the position of the cluster's equilibrium geometry in the respective electronic state.

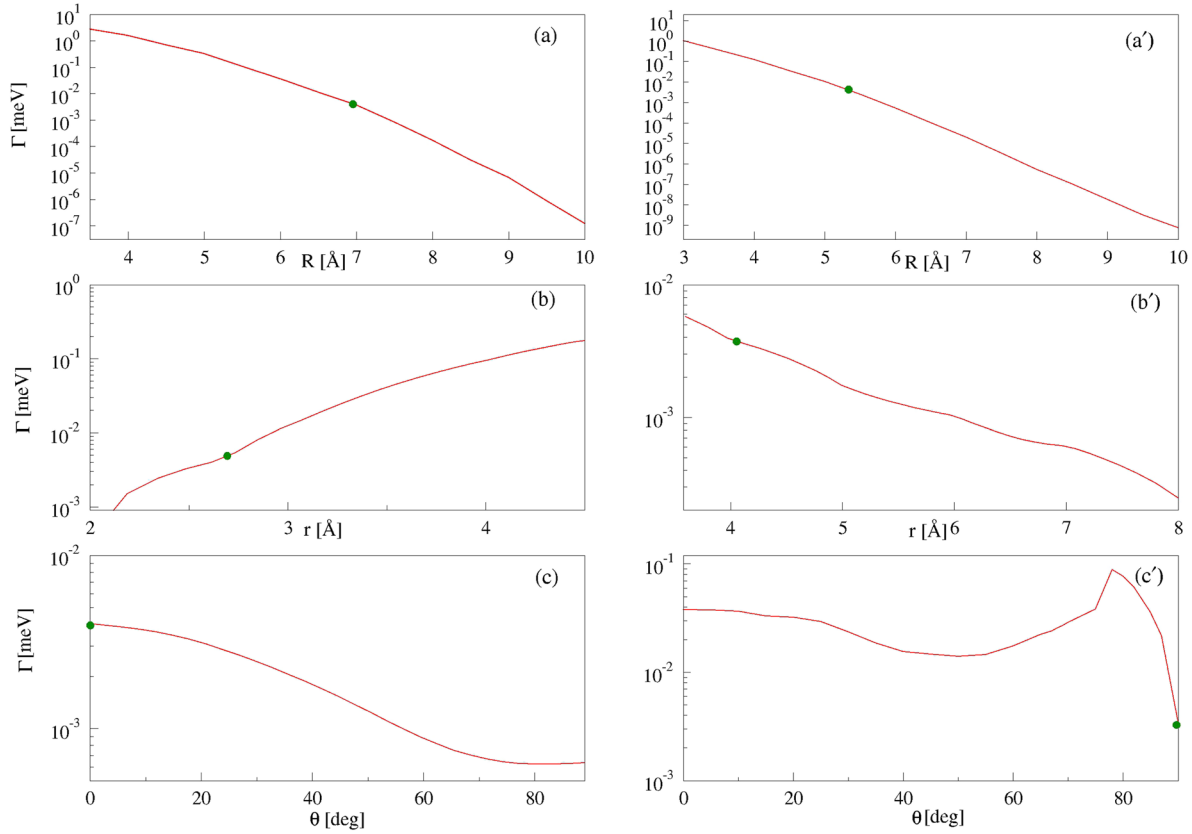

FIG. 5. ETMD widths of the $He^+Li_2(^1\Sigma_g^+)$ (left panels) and $He^+Li_2(^3\Sigma_u^+)$ (right panels) states along different cuts of the respective PES. The cuts go through the point corresponding to the equilibrium geometry of the respective initial state (see Table II) and are obtained by keeping two Jacobi coordinates constant, while varying the third. [(a) and (a′)] R is varied, [(b) and (b′)] r is varied, and [(c) and (c′)] θ is varied. The green dots denote the location of the equilibrium geometries on the respective cut.

mass of Li_2 is very large (R ≫ r). However, the values of R used in constructing the cuts are not large enough and the width depends on θ. This dependence is defined predominantly by the distance between He^+ and the valence electron density of Li_2. The width of the $He^+Li_2(^1\Sigma_g^+)$ state decreases monotonically by a factor of 7 when the angle is increased from 0 to $\pi/2$, i.e., when He^+ is moved from the linear to the T-shaped geometry. It can be explained by the increasing distance between the He^+ ion and the valence electron density of Li_2, which is located on the molecular axis between the two Li atoms.

The behavior of the width of the $He^+Li_2(^3\Sigma_u^+)$ state with θ is markedly different. It decreases up to $\theta = 40°$ before starting to increase, peaking at $\theta = 80°$ and sharply falling off at $\theta = 90°$. The overall change in Γ between 0° and 90° is factor 10 and is comparable to the drop in the width in the previous case. Its non-monotonic behavior can be understood if we remember that the $He^+Li_2(^3\Sigma_u^+)$ PES intersects the PES of the $He^*Li_2^+(^3\Sigma_u^+)$ resonance state. The latter resonance decays into the same final state via an excitation transfer ionization mechanism and has a larger decay width. The two surfaces remain close to each other and interact when R and r are kept at the equilibrium values of the initial state and while θ is between 40° and 80°. This causes the observed behavior of the width of the $He^+Li_2(^3\Sigma_u^+)$ state. Computing the ETMD width along a similar cut at larger R away from the crossing showed a monotonically decreasing width similar to the one in Fig. 5(c).

Although it is coupled to the ETMD state, we can neglect the $He^*Li_2^+(^3\Sigma_u^+)$ state in calculating the nuclear dynamics and ETMD spectra. The crossing points fall on the repulsive wall of the respective PES, and the decay width is low at the corresponding geometries. Therefore, even if this state is populated in the photoionization step, or in the following nuclear dynamics, it will dissociate prior to the decay. Moreover, the coupling term involves electron transfer integrals and should be small at the values of R involved so that no significant population of this state can be expected. The situation might become quite different for heavier alkali dimers, where the crossing should occur at a shorter distance R due to their lower ionization potentials.

The conclusion we may draw is that the largest impact on the ETMD rate will be produced by the motion along the coordinate R. However, the variation of the rate with r and θ is also non-negligible and can reach an order of magnitude.

D. Qualitative estimates of ETMD electron spectra

To obtain accurate ETMD spectra, one needs to propagate vibrational wavepackets on the decaying state PES.[21] However, a qualitative estimate of the electron spectra can be obtained by considering the PES and the decay widths alone. The procedure is easily visualized in one dimension. There the initial wavepacket is produced by vertically transferring the vibrational wavefunction of the initial weakly bound electronic state to the potential energy curve of the decaying state. Since ETMD is initiated by the ionization of one constituent, the potential minimum in the decaying state is deeper and is located at a shorter interatomic distance than in the initial state. Moreover, in the van der Waals clusters, ETMD is slow at the geometries in the Franck-Condon region. Therefore, the wavepacket propagates toward shorter interatomic distances during the decay. If no ETMD channels are closed at the interatomic distances where dynamics take place, then the decay rate reaches its maximum at the inner turning point of the potential. Since the classical velocity is zero at this point, the system spends a long time there, and the majority of the decay events take place in its vicinity.[21] Consequently, the electron spectrum can be estimated as the energy difference between the decaying and final PECs taken at the turning point's coordinate.

We can use similar reasoning to estimate ETMD electron spectra in a multidimensional potential. For the $HeLi_2(^1\Sigma_g^+)$ state, we note that the Li_2 bond does not break during the dynamics so that to simplify matters we keep the coordinate r constant at its equilibrium value in the decaying state (2.9 Å). The point on the decaying state PES reached vertically from the respective equilibrium geometry of the initial state gives us the initial vibrational energy E_0. For each value of θ, we find a classical inner turning point $R(\theta)$ corresponding to E_0. The plot of $R(\theta)$ and the corresponding ETMD widths are shown in Figs. 6(a) and 6(b). The turning points correspond to the geometries at which the He^+ ion collides with the Li_2 molecule and is reflected back. It follows from the plots that the He^+ ion can approach Li_2, the nearest at the T-shaped geometry. At this turning point, it is closest to the valence electron density of Li_2 which leads to a strong increase in Γ. Indeed, the latter changes from 2.5 meV for the turning point at $\theta = 0$ to 20 meV for the one at $\theta = \pi/2$. The ETMD lifetimes at these points lie between 270 fs and 35 fs and are 3 to 4 orders of magnitude shorter than the lifetimes in the Franck-Condon region. The electron spectrum obtained as the energy difference between the decaying and final states at the turning points is shown in Fig. 6(c). It lies in the region between 6.8 eV and 7.8 eV.

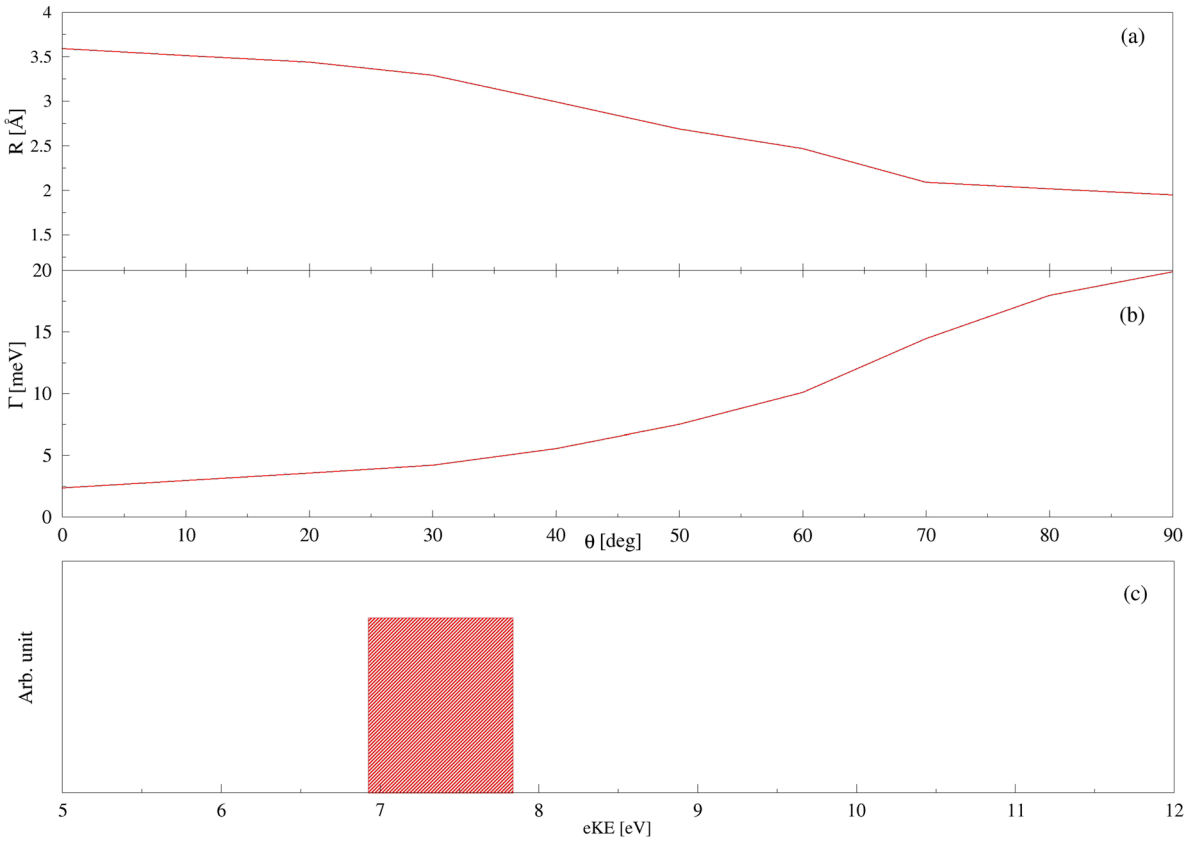

FIG. 6. (a) The locus of classical turning points on the $He^+Li_2(^1\Sigma_g^+)$ PES obtained by keeping the coordinate r at its equilibrium value in the decaying state (2.9 Å). (b) ETMD widths corresponding to the turning points in (a). (c) ETMD electron spectra obtained under an assumption that the decay occurs only at the turning points in (a).

In the $He^+Li_2(^3\Sigma_u^+)$ state, the weak Li_2 bond breaks during the dynamics which accompanies the decay so that the global minimum is the linear Li–He^+–Li configuration. Since both the center of the initial wavepacket and the global minimum of the decaying state lie at $\theta = \pi/2$, to estimate the ETMD electron spectrum, we keep θ constant at this value. Defining the initial vibrational energy in the similar way as in the case above, we find the positions of the turning points [Fig. 7(a)] and the corresponding ETMD width [Fig. 7(b)]. The turning points again correspond to the geometries at which the He^+ ion collides with Li_2. They show in this case a bigger variation in the value of R as is the case of the $He^+Li_2(^1\Sigma_g^+)$ state. Consequently, it produces a larger variation in the values of Γ which reaches three orders of magnitude (3.2 meV–0.0015 meV). Moreover, we see that although the decay will be accelerated due to nuclear dynamics, the expected effect will be weaker than in the case of the $He^+Li_2(^1\Sigma_g^+)$ state. The corresponding electron spectrum shown in Fig. 7(c) lies between 8 eV and 10.5 eV. It is shifted to higher energies and broadened compared to the spectrum of the $He^+Li_2(^1\Sigma_g^+)$ state. The shift is mostly due to the higher energy of the $Li_2(^3\Sigma_u^+)$ fragment relative to the $Li_2(^1\Sigma_g^+)$ ground state, which is close to 1 eV in the isolated molecule. The broadening is mostly due to the large variation in the Li–Li distance among the turning points. Indeed, this is the coordinate along which the energy in the final $HeLi^+Li^+$ varies the strongest.

For comparison, we also computed the minimum energy path on the PES of the $HeLi_2(^3\Sigma_u^+)$ state when $\theta = \pi/2$ [see Fig. 7(a′)]. Along this path, the movement of He^+ toward Li_2 does not at first perturb the latter. At shorter values of R, the Li–Li distance increases until He^+ reaches the global minimum between the Li atoms. The decay width grows exponentially at first and then starting from R = 2 Å, it reaches a plateau at 1.3 meV [see Fig. 7(b′)]. The electron spectrum is computed as the energy difference between the decaying and the final PES for all geometries corresponding to the path. It appears as a narrow band between 9.5 eV and 11 eV [see Fig. 7(c′)]. The shift to higher energies compared with the spectrum obtained at inner turning points is due to the larger Li–Li distance and consequently lower energy in the final state. The system will follow the minimum energy path, for example, if the vibrational energy is fast

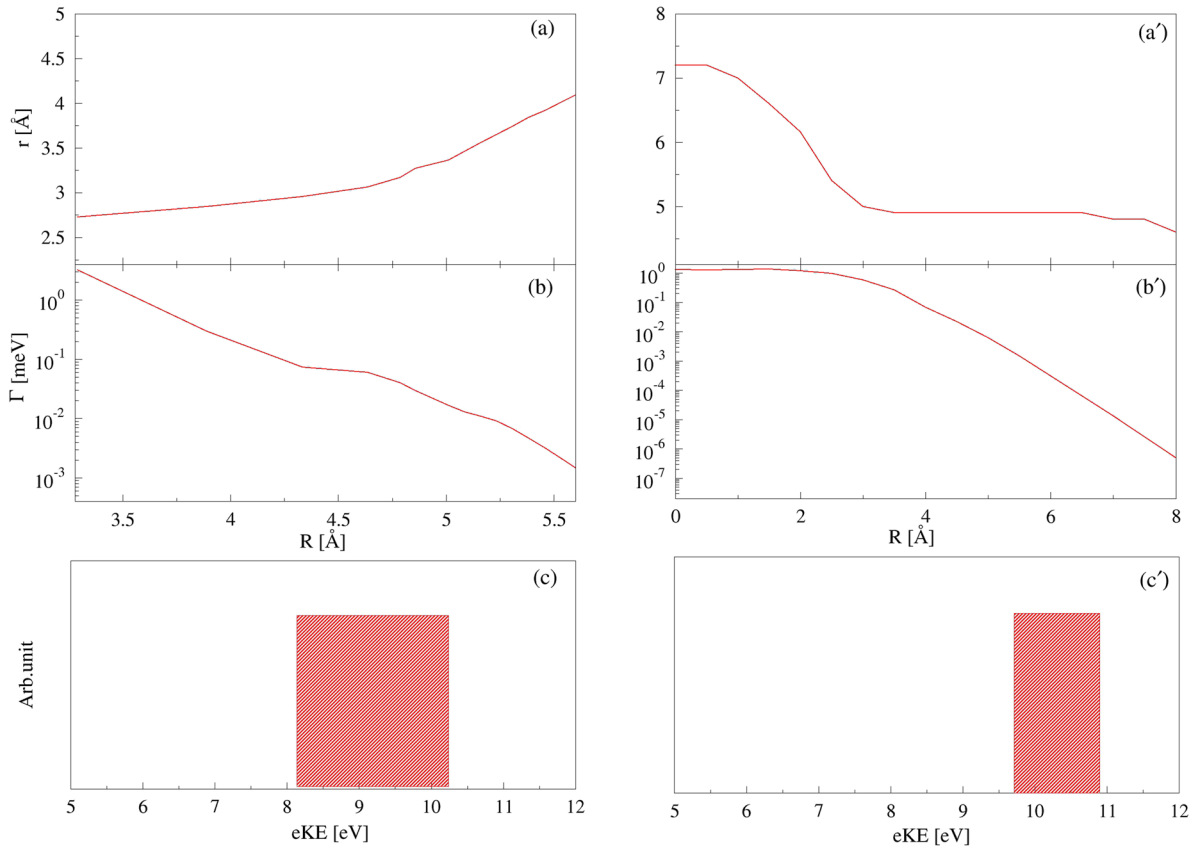

FIG. 7. (a) The locus of classical turning points on the $He^+Li_2(^3\Sigma_u^+)$ PES obtained by keeping the coordinate $\theta = \pi/2$. (b) ETMD widths corresponding at the turning points in (a). (c) ETMD electron spectra obtained under an assumption that the decay occurs only at the turning points in (a). (a′) Minimum energy path on the $He^+Li_2(^3\Sigma_u^+)$ PES obtained by keeping the coordinate $\theta = \pi/2$. (b′) ETMD widths at the coordinates on the minimum energy path. (c′) Obtained under an assumption that the decay occurs only on the minimum energy path.

dissipated. This scenario can be realized in the He droplet where the energy is transferred to the neutral He atoms and used to evaporate them.

IV. CONCLUSIONS

In this article, we carried out a preliminary investigation of the ETMD process in the $HeLi_2$ cluster which is induced by ionizing the He atom. We computed the potential energy surfaces of the initial $HeLi_2(^1\Sigma_g^+)$ and $HeLi_2(^3\Sigma_u^+)$ states, decaying $He^+Li_2(^1\Sigma_g^+)$ and $He^+Li_2(^3\Sigma_u^+)$ states, and the final $HeLi^+Li^+$ state. Moreover, we computed the ETMD widths for both decaying states. We analyzed the potential energy surfaces and the decay widths and estimated ETMD electron spectra. The computed PES and widths will be used in a forthcoming publication where quantum dynamics methods are applied to study the impact of multimode nuclear dynamics on the ETMD process and observable spectra.

However, some conclusions can be already drawn by considering the electronic data alone. First, the potential energy surfaces of the initial and decaying states are determined by the interaction between the He moiety and the valence electrons of Li_2. Since He is repulsed by electrons and He^+ is strongly attracted by them, the PESs corresponding to the initial and decaying states have widely different structures. The decaying states are stronger bound and have different symmetries of their equilibrium geometries. This together with the observation that the ETMD lifetimes at the initial states' equilibrium geometries are as long as 200 ps means that excitation to the decaying state will be followed by nuclear dynamics. Moreover, since the valence electron density and the bond strength in the $Li_2(^3\Sigma_u^+)$ and $Li_2(^3\Sigma_u^+)$ fragments differ, the dynamics and the decay in the two decaying states will be profoundly different.

The Li–Li bond is strong in the $HeLi_2(^1\Sigma_g^+)$ state; therefore, the dynamics are of the He^+ ion interacting with the Li_2 molecule. We found the points at which the classical velocity was zero and the ETMD lifetimes were many orders of magnitude shorter than in the Franck-Condon region (35–270 fs). Previous experience showed that the majority of the decay events occur at such classical turning points and the electron spectrum can be well estimated by taking the difference between the energies of the decaying and final states. The spectrum which corresponds to the decay in the $He^+Li_2(^1\Sigma_g^+)$ state appears as a band between 6.8 eV and 7.8 eV. The van der Waals Li–Li bond in the $He^+Li_2(^3\Sigma_u^+)$ state is very weak and is expected to break during the nuclear dynamics. The electron spectrum estimated from the classical turning points lies between 8 eV and 10.5 eV.

The above two spectra differ, reflecting the difference in the electronic structure of the two decaying states and different vibrational modes which are mostly active in the dynamics accompanying the decay. Full quantum dynamics calculations in $HeLi_2$, which use the electronic properties presented in this paper as the input, will be published later. They should allow detailed understanding of the electronic decay and electron spectra in a multidimensional vibrating system. Moreover, since ETMD in the $HeLi_2$ cluster can be viewed as a model for ETMD in Li_2 doped He droplets, we hope that the current and forthcoming results will be useful in identifying the signature of this process in the electron spectroscopy experiments.

SUPPLEMENTARY MATERIAL

See supplementary material for the potential energy surfaces and electronic decay widths. Details of the file structure and content are provided in the accompanying readme file.

ACKNOWLEDGMENTS

The authors would like to thank Markus Schröder and Vasili Stumpf for their help with the computations, and Aaron LaForge and Marcel Mudrich for numerous discussions and suggestions. Financial support by the European Research Council (ERC) (Advanced Investigator Grant No. 692657) and the Deutsche Forschungsgemeinschaft (Grant No. DFG-FOR 1789) is gratefully acknowledged.

REFERENCES

[1] J. P. Toennies and A. F. Vilesov, Angew. Chem., Int. Ed. **43**, 2622 (2004).
[2] A. Mauracher, O. Echt, A. Ellis, S. Yang, D. Bohme, J. Postler, A. Kaiser, S. Denifl, and P. Scheier, Phys. Rep. **751**, 1 (2018).
[3] M. Y. Choi, G. E. Douberly, T. M. Falconer, W. K. Lewis, C. M. Lindsay, J. M. Merritt, P. L. Stiles, and R. E. Miller, Int. Rev. Phys. Chem. **25**, 15 (2006).
[4] M. Hartmann, A. Lindinger, J. Toennies, and A. F. Vilesov, Chem. Phys. **239**, 139 (1998).
[5] M. Hartmann, A. Lindinger, J. P. Toennies, and A. F. Vilesov, Phys. Chem. Chem. Phys. **4**, 4839 (2002).
[6] B. Najjari, A. B. Voitkiv, and C. Müller, Phys. Rev. Lett. **105**, 153002 (2010).
[7] F. Trinter, J. B. Williams, M. Weller, M. Waitz, M. Pitzer, J. Voigtsberger, C. Schober, G. Kastirke, C. Müller, C. Goihl, P. Burzynski, F. Wiegandt, R. Wallauer, A. Kalinin, L. P. H. Schmidt, M. Schöffler, Y.-C. Chiang, K. Gokhberg, T. Jahnke, and R. Dörner, Phys. Rev. Lett. **111**, 233004 (2013).
[8] G. Jabbari, S. Klaiman, Y.-C. Chiang, F. Trinter, T. Jahnke, and K. Gokhberg, J. Chem. Phys. **140**, 224305 (2014).
[9] M. Mudrich and F. Stienkemeier, Int. Rev. Phys. Chem. **33**, 301 (2014).
[10] A. Scheidemann, B. Schilling, and J. P. Toennies, J. Phys. Chem. **97**, 2128 (1993).
[11] W. K. Lewis, C. M. Lindsay, R. J. Bemish, and R. E. Miller, J. Am. Chem. Soc. **127**, 7235 (2005).
[12] W. K. Lewis, C. M. Lindsay, and R. E. Miller, J. Chem. Phys. **129**, 201101 (2008).
[13] D. Buchta, S. R. Krishnan, N. B. Brauer, M. Drabbels, P. O'Keeffe, M. Devetta, M. Di Fraia, C. Callegari, R. Richter, M. Coreno, K. C. Prince, F. Stienkemeier, R. Moshammer, and M. Mudrich, J. Phys. Chem. A **117**, 4394 (2013).
[14] N. Saito, Y. Morishita, I. H. Suzuki, S. D. Stoychev, A. I. Kuleff, L. S. Cederbaum, X.-J. Liu, H. Fukuzawa, G. Prümper, and K. Ueda, Chem. Phys. Lett. **441**, 16 (2007).
[15] A. Hans, V. Stumpf, X. Holzapfel, F. Wiegandt, P. Schmidt, C. Ozga, P. Reiß, L. B. Ltaief, C. Küstner-Wetekam, T. Jahnke, A. Ehresmann, P. V. Demekhin, K. Gokhberg, and A. Knie, New J. Phys. **20**, 012001 (2018).
[16] J. Zobeley, R. Santra, and L. S. Cederbaum, J. Chem. Phys. **115**, 5076 (2001).
[17] K. Sakai, S. Stoychev, T. Ouchi, I. Higuchi, M. Schöffler, T. Mazza, H. Fukuzawa, K. Nagaya, M. Yao, Y. Tamenori, A. I. Kuleff, N. Saito, and K. Ueda, Phys. Rev. Lett. **106**, 033401 (2011).
[18] M. Förstel, M. Mucke, T. Arion, A. M. Bradshaw, and U. Hergenhahn, Phys. Rev. Lett. **106**, 033402 (2011).
[19] D. You, H. Fukuzawa, Y. Sakakibara, T. Takanashi, Y. Ito, G. G. Maliyar, K. Motomura, K. Nagaya, T. Nishiyama, K. Asa, Y. Sato, N. Saito, M. Oura, M. Schöffler, G. Kastirke, U. Hergenhahn, V. Stumpf, K. Gokhberg, A. I. Kuleff, L. S. Cederbaum, and K. Ueda, Nat. Commun. **8**, 14277 (2017).
[20] I. Unger, R. Seidel, S. Thürmer, M. N. Pohl, E. F. Aziz, L. S. Cederbaum, E. Muchová, P. Slavíček, B. Winter, and N. V. Kryzhevoi, Nat. Chem. **9**, 708 (2017).
[21] V. Stumpf, S. Scheit, P. Kolorenč, and K. Gokhberg, Chem. Phys. **482**, 192 (2017).
[22] I. B. Müller and L. S. Cederbaum, J. Chem. Phys. **122**, 094305 (2005).

[23]V. Stumpf, K. Gokhberg, and L. S. Cederbaum, Nat. Chem. **8**, 237 (2016).
[24]V. Stumpf, N. V. Kryzhevoi, K. Gokhberg, and L. S. Cederbaum, Phys. Rev. Lett. **112**, 193001 (2014).
[25]A. C. LaForge, V. Stumpf, K. Gokhberg, J. von Vangerow, F. Stienkemeier, N. V. Kryzhevoi, P. O'Keeffe, A. Ciavardini, S. R. Krishnan, M. Coreno, K. C. Prince, R. Richter, R. Moshammer, T. Pfeifer, L. S. Cederbaum, and M. Mudrich, Phys. Rev. Lett. **116**, 203001 (2016).
[26]S. Denifl, F. Zappa, I. Mähr, F. Ferreira da Silva, A. Aleem, A. Mauracher, M. Probst, J. Urban, P. Mach, A. Bacher, O. Echt, T. Märk, and P. Scheier, Angew. Chem., Int. Ed. **48**, 8940 (2009).
[27]S. Denifl, F. Zappa, I. Mähr, A. Mauracher, M. Probst, J. Urban, P. Mach, A. Bacher, D. K. Bohme, O. Echt, T. D. Märk, and P. Scheier, J. Chem. Phys. **132**, 234307 (2010).
[28]V. Stumpf, P. Kolorenč, K. Gokhberg, and L. S. Cederbaum, Phys. Rev. Lett. **110**, 258302 (2013).
[29]F. Stienkemeier, J. Higgins, W. E. Ernst, and G. Scoles, Phys. Rev. Lett. **74**, 3592 (1995).
[30]F. Stienkemeier, W. E. Ernst, J. Higgins, and G. Scoles, J. Chem. Phys. **102**, 615 (1995).
[31]M. Mudrich, O. Bünermann, F. Stienkemeier, O. Dulieu, and M. Weidemüller, Eur. Phys. J. D **31**, 291 (2004).
[32]M. Musiał and S. A. Kucharski, J. Chem. Theory Comput. **10**, 1200 (2014).
[33]J. Higgins, C. Callegari, J. Reho, F. Stienkemeier, W. E. Ernst, M. Gutowski, and G. Scoles, J. Phys. Chem. A **102**, 4952 (1998).
[34]F. Lackner, J. Poms, G. Krois, J. V. Pototschnig, and W. E. Ernst, J. Phys. Chem. A **117**, 11866 (2013).
[35]E. Bodo, F. Gianturco, and E. Yurtsever, J. Low Temp. Phys. **138**, 259 (2005).
[36]O. Bünermann and F. Stienkemeier, Eur. Phys. J. D **61**, 645 (2011).
[37]S. Bovino, E. Coccia, E. Bodo, D. Lopez-Durán, and F. A. Gianturco, J. Chem. Phys. **130**, 224903 (2009).
[38]M. W. Schmidt, K. K. Baldridge, J. A. Boatz, S. T. Elbert, M. S. Gordon, J. H. Jensen, S. Koseki, N. Matsunaga, K. A. Nguyen, S. Su, T. L. Windus, M. Dupuis, and J. A. Montgomery, J. Comput. Chem. **14**, 1347 (1993).
[39]P. Piecuch, S. A. Kucharski, K. Kowalski, and M. Musiał, Comput. Phys. Commun. **149**, 71 (2002).
[40]A. J. C. Varandas and J. Brandão, Mol. Phys. **57**, 387 (1986).
[41]M. Fuchs and J. P. Toennies, J. Chem. Phys. **85**, 7062 (1986).
[42]P. Piecuch and M. Włoch, J. Chem. Phys. **123**, 224105 (2005).
[43]J. N. Bardsley, J. Phys. B: At. Mol. Phys. **1**, 349 (1968).
[44]K. Kaufmann, W. Baumeister, and M. Jungen, J. Phys. B: At. Mol. Phys. **22**, 2223 (1989).
[45]V. Averbukh and L. S. Cederbaum, J. Chem. Phys. **123**, 204107 (2005).
[46]U. Fano, Phys. Rev. **124**, 1866 (1961).
[47]H. Feshbach, Ann. Phys. **5**, 357 (1958).
[48]H. Feshbach, Ann. Phys. **19**, 287 (1962).
[49]F. Müller-Plathe and G. Diercksen, Phys. Rev. A **40**, 696 (1989).
[50]J. Schirmer, L. S. Cederbaum, and O. Walter, Phys. Rev. A **28**, 1237 (1983).
[51]F. Mertins and J. Schirmer, Phys. Rev. A **53**, 2140 (1996).
[52]F. Aquilante, L. De Vico, N. Ferré, G. Ghigo, P.-Å. Malmqvist, P. Neogrády, T. B. Pedersen, M. Pitoňák, M. Reiher, B. O. Roos, L. Serrano-Andrés, M. Urban, V. Veryazov, and R. Lindh, J. Comput. Chem. **31**, 224 (2010).
[53]T. Miteva, S. Klaiman, E. V. Gromov, and K. Gokhberg, J. Chem. Phys. **140**, 204320 (2014).
[54]P. Jasik, J. Wilczyński, and J. E. Sienkiewicz, Eur. Phys. J.: Spec. Top. **144**, 85 (2007).